

1 **Structure of the connexin-43 gap junction channel in a**
2 **putative closed state**

3

4 Chao Qi^{1,2,#}, Silvia Acosta-Gutierrez^{3,#}, Pia Lavriha^{1,2}, Alaa Othman⁴, Diego Lopez-
5 Pigozzi^{5,6}, Erva Bayraktar⁶, Dina Schuster^{1,2,4}, Paola Picotti⁴, Nicola Zamboni⁴, Mario
6 Bortolozzi^{5,6}, Francesco L. Gervasio^{7,8,9*} and Volodymyr M. Korkhov^{1,2*}

7

8 ¹ Institute of Molecular Biology and Biophysics, ETH Zurich, Switzerland

9 ² Laboratory of Biomolecular Research, Paul Scherrer Institute, Villigen, Switzerland

10 ³ Institute for the Physics of Living Systems, Institute of Structural and Molecular Biology,
11 and Department of Chemistry. University College London, London, UK

12 ⁴ Institute of Molecular Systems Biology, ETH Zurich, Switzerland

13 ⁵ Department of Physics and Astronomy “G. Galilei”, University of Padova, Padua, Italy

14 ⁶ Veneto Institute of Molecular Medicine (VIMM), Padua, Italy

15 ⁷ Department of Chemistry, University College London, WC1E 6BT London, UK

16 ⁸ School of Pharmaceutical Sciences, University of Geneva, CH-1211 Geneva, Switzerland

17 ⁹ ISPSO, University of Geneva, CH-1211 Geneva, Switzerland

18

19 * Corresponding authors: francesco.gervasio@unige.ch, volodymyr.korkhov@psi.ch

20 # These authors contributed equally

21

22 **Abstract**

23 Gap junction channels (GJCs) mediate intercellular communication by connecting two
24 neighboring cells and enabling direct exchange of ions and small molecules. Cell coupling via
25 connexin-43 (Cx43) GJCs is important in a wide range of cellular processes in health and
26 disease¹⁻³, yet the structural basis of Cx43 function and regulation has not been determined
27 until now. Here we describe the structure of a human Cx43 GJC solved by cryo-EM and single
28 particle analysis at 2.26 Å resolution. The pore region of Cx43 GJC features several lipid-like
29 densities per Cx43 monomer, located close to a putative lateral access site at the monomer
30 boundary. We found a previously undescribed conformation on the cytosolic side of the pore,
31 formed by the N-terminal domain and the transmembrane helix 2 of Cx43 and stabilized by a
32 small molecule. Structures of the Cx43 GJC and hemichannels in nanodiscs reveal a similar
33 gate arrangement. The features of the Cx43 GJC and hemichannel cryo-EM maps and the
34 channel properties revealed by molecular dynamics simulations suggest that the captured states
35 of Cx43 are consistent with a closed state.

36

37 **Introduction**

38 Gap junction (GJ) mediated intercellular communication is one of the major pathways of
39 information exchange between the cells. GJs are specialized regions of the plasma membrane
40 at the cell-cell interface that link two adjacent cells and establish their metabolic and electrical
41 coupling⁴. Connexins are the building blocks of the GJ channels (GJC)s which belong to a
42 group of large-pore channels. This group includes a number of structurally related (innexins,
43 pannexins, LRRC8) and unrelated proteins (CALHM)⁵. A total of 21 connexin genes have
44 been identified in the human genome⁶. The 43 kDa connexin-43 (Cx43, gene name *GJA1*) was
45 identified as a major constituent of rat heart GJs in 1987⁷, and it is arguably one of the most
46 extensively studied connexins. Like all connexin homologues, Cx43 monomers assemble into
47 hexameric hemichannels (HCs), also known as connexons. HCs that reach the plasma
48 membrane of one cell may interact with their counterparts on the neighboring cell, forming
49 GJC>s, typically organized into hexagonal arrays at the intercellular interface⁸. GJC>s enable
50 direct metabolic and electric coupling between the cells, facilitating the passage of ions, small
51 molecules, metabolites, peptides and other cellular components below a size threshold of
52 approximately 1.5 kDa⁹. GJC>s formed by Cx43 are crucial for a wide range of physiological
53 processes, from propagation of heart action potentials³ to maintenance of neuro-glial
54 syncytium² and skin wound healing¹. The clinical importance of Cx43 is highlighted by
55 mutations linked to several genetic disorders, such as oculodentodigital dysplasia (ODDD)¹⁰-
56 hypoplastic left heart syndrome 1¹³, Hallermann-Streiff syndrome¹⁴, atrioventricular septal
57 defect 3¹³, etc., and by recognition of the protein as a drug target for treatment of cancer, skin
58 wounds, eye injury and inflammation and cardiac arrhythmias (reviewed by Laird and Lampe
59⁹).

60 Much of what we know today about the molecular biology, electrophysiological properties and
61 regulation of connexin gap junctions has been derived from the studies on Cx43 (reviewed in
62¹⁵). Early attempts to characterize the structure of Cx43 using cryo-electron microscopy (cryo-
63 EM) of 2D crystals produced low resolution reconstructions¹⁶. More recently, several
64 homologous connexin GJC>s and HCs have been structurally characterized at high resolution,
65 using X-ray crystallography and cryo-EM. The structures of Cx26¹⁷ and Cx46/50 GJC>s^{18,19},
66 together with the recent structure of Cx31.3 HC²⁰ provided deep insights into the shared
67 structural features of the connexin channels. These structures hint at the role of the N-terminal
68 domain (NTD) in molecular gating of GJC>s and HCs, with several conformations of the NTD
69 observed in different connexin homologues¹⁸⁻²⁰. Additionally, biochemical evidence points to
70 the roles in channel gating played by the link between Cx43 intracellular loop and the C-
71 terminal region^{21,22}. However, despite the availability of this evidence, the molecular
72 determinants of intracellular connexin channel gating remain unclear. To shed light on the
73 structural basis of Cx43 gating, we set out to determine its structure by cryo-EM and to analyse
74 its dynamics with molecular dynamics (MD) simulations.

75

76 **Results**

77 **Structures of Cx43 GJC and HC in detergent micelles and in nanodiscs.** Our Cx43
78 expression system was tested using electrophysiology in HeLa cells (Extended Data Fig. 1a-d). The experiments confirmed the functionality of Cx43 GJC>s expressed in transfected cells.
79 For large-scale protein expression, Cx43 featuring a C-terminal HRV3C-YFP-twinStrep tag,
80 was expressed in adherent mammalian cells (HEK293F) using transient transfection method.
81 The produced protein was purified using affinity and size exclusion chromatography in
82 digitonin (Extended Data Fig. 2a-c) and flash frozen on cryo-EM grids. The coomassie-stained
83 SDS PAGE gel bands of the purified protein (Extended Data Fig. 2c) are consistent with the
84 western blot analysis (Extended Data Fig. 2d) of the expressed untagged Cx43. The grids were
85

86 subjected to single particle cryo-EM analysis (Extended Data Fig. 3), yielding the final 3D
87 reconstruction at 2.26 Å resolution (Fig. 1a, Extended Data Fig. 3-4).

88 The overall architecture of the protein complex resembles that observed with other connexin
89 GJCs, with two hemichannels (connexons) from adjacent plasma membrane regions coupled
90 to form a full GJC (Fig. 1a-b). The exterior of the channel is decorated by several ordered
91 detergent and/or lipid-like density elements (Fig. 1a-b), reminiscent of the previously observed
92 lipids bound at the protein-bilayer interface in other connexins¹⁹. In the case of Cx43, the lipid-
93 like densities appear to decorate the protein-lipid bilayer interface at both the inner and the
94 outer leaflet of the membrane. Comparison of the Cx43 monomers to the available structures
95 of Cx26 and Cx46 GJCs and the Cx31.3 HC revealed a major difference in the NTD
96 arrangement in these channels (Fig. 1c-d). The conformation of the NTD in the Cx31.3 HC
97 structure appears to be the closest to that in Cx43 GJC. Analysis of the tryptic peptides revealed
98 that most of the protein lacks the residue M1 (Extended Data Fig. 5), and thus the model was
99 built starting with G2.

100 To ascertain that the conformation of Cx43 GJC is not induced by the detergent present in the
101 sample, e.g. through detergent binding at specific sites on the protein surface, we removed the
102 detergent and reconstituted the protein into MSP2N2 nanodiscs, using 1-palmitoyl-2-oleoyl-
103 glycero-3-phosphocholine (POPC) as a mimic for the native lipid environment. The
104 reconstituted protein was subjected to the same imaging and analysis workflow as Cx43 GJC
105 in digitonin. The 2D classes of the MSP2N2-reconstituted Cx43 showed features consistent
106 with a mixture of GJCs and HC. Processing of the corresponding particles resulted in 3D
107 reconstructions of the Cx43 GJC at 2.95 Å resolution (Extended Data Fig. 6, 8) and HC in
108 nanodiscs at 3.98 Å resolution (Fig. 1e-f, Extended Data Fig. 7, 8). The GJCs in detergent and
109 in nanodiscs are nearly identical, with an RMSD of 0.97 Å between the aligned Cx43
110 monomers (Fig. 1g, Extended Data Fig. 9a). Although the differences between the HC in
111 nanodisc and the GJC are more pronounced (Extended Data Fig. 9a), the conformation of the
112 cytosolic region and the NTD is highly conserved (Fig. 1g).

113 **Conformation of the Cx43 gate region.** The reconstructed gate region of Cx43 shows several
114 narrow openings connecting the pore vestibule and the pore interior: a single ~6-7 Å wide
115 central opening and six adjacent openings of similar dimensions (Fig. 2a-b). This arrangement
116 of the gate region is distinct from any of the previously observed states of connexin GJCs or
117 HCs. This particular gate conformation is established through an interplay of two structural
118 elements: the NTD and the TM2 (Fig. 2c-d). The NTD of Cx43 is arranged near parallel to the
119 membrane plane, in a centre-oriented conformation (Fig. 2c). The HC of Cx31.3 assembles in
120 a similar manner, with a well-ordered NTD resolved by cryo-EM (Fig. 2c-d). However, the
121 TM2 region of Cx31.3 forms a tight seal with the NTD (Fig. 2e). In contrast, the TM2 of Cx43
122 is shifted away from the pore centre, creating six openings (Fig. 2f). Alignment of the
123 protomers of Cx43 and Cx31.3 showed an RMSD of 1.78 Å (using cealign in PyMol). In
124 contrast, the RMSD value for the region corresponding to the NTD and TM2 was 5.675 Å
125 (calculated using rms_cur in PyMol, with the residue range selections of 2-47 and 2-45 for the
126 aligned protomers of Cx43 and Cx31.3, respectively), further confirming that these two regions
127 differ substantially between Cx43 and Cx31.3. The arrangement of the Cx43 NTD appears to
128 be stabilized by a small molecule: a density element likely corresponding to a bound small
129 molecule is present within this region (referred to as the “NTD lipid site”), wedged between
130 the adjacent NTDs (Fig. 2g). Thus, although the conformation of the Cx43 gate features an
131 opening, this site is blocked by a yet unidentified small molecule (which we refer to as “lipid-
132 N”).

133 While a direct comparison of the Cx43 gating regions of the Cx43 and Cx31.3 HCs is possible
134 (Extended Data Fig. 9c), the recently determined 3D reconstruction of the Cx26 mutant N176Y

135 was not accompanied by a new atomic model²³. Instead the study reporting this reconstruction
136 compared the density map with an HC model from a Cx26 GJC structure (PDB ID: 5ERA)²⁴.
137 As this model lacks the NTD, any comparisons of the gating region in the Cx43 HC with that
138 in the Cx26 HC are presently limited (Extended Data Fig. 9d).

139 In addition to the lipid-N molecules stabilizing the NTD arrangement, the cryo-EM density of
140 Cx43 GJC features several well resolved densities inside the pore region (lipid-1 and lipid-2,
141 Fig. 2h). These elements likely correspond to bound sterol molecules, such as cholesterol co-
142 purified with the protein from the mammalian cells or cholesterol hemisuccinate (CHS) added
143 to the solubilization mixture during protein extraction from the membrane. Similar densities
144 are present in the Cx43 GJC reconstruction in nanodiscs, in the absence of detergent molecules
145 (Extended Data Fig. 10a). Additionally, it is noteworthy that the annular lipid densities are
146 conserved in both the detergent-solubilized and the nanodisc-reconstituted Cx43 GJCs,
147 indicating that the protein-lipid interface of Cx43 features sites where ordered lipid molecules
148 may bind (Extended Data Fig. 10b). The functional significance of the ordered annular lipids
149 for the channel activity and for GJ plaque assembly remains to be carefully investigated.

150 Identification of the lipid-like molecules bound to Cx43 is a significant challenge. Despite the
151 high overall resolution of the 3D reconstruction of the Cx43 GJC (2.26 Å resolution in
152 detergent and 2.95 Å in nanodisc; Extended Data Fig. 3, 6), the cryo-EM map features in
153 regions corresponding to the lipid densities are insufficient to assign the lipid identity
154 unambiguously. To determine the identities of these lipids experimentally, we performed
155 lipidomic analysis of the organic extracts prepared from the purified Cx43 samples and
156 compared them to the mock control (extracts of prepared from eluates of the purification
157 procedure using cells that do not overexpress the protein as starting material). The results
158 showed that several types of phospholipids, as well as cholesterol were present in both samples.
159 The only lipid-like compound specifically enriched in the purified sample was
160 dehydroepiandrosterone (DHEA; Extended Data Fig. 10c). DHEA is a most abundantly
161 expressed neurosteroid known to modulate ligand-gated ion channels, such as GABA_A²⁵ or
162 NMDA and AMPA receptors²⁶. Although we are presently not able to conclusively state that
163 DHEA corresponds to any of the densities present in our reconstruction, its enrichment in the
164 sample is an interesting observation that deserves detailed future investigations. While the
165 density corresponding to lipid-N may correspond to DHEA (Extended Data Fig. 4e), it is also
166 possible that this density corresponds to a larger molecule that is only partially ordered.

167 **Cx43 junction interface.** As in other connexins, the Cx43 GJC interface is formed by two
168 extracellular loops, ECL1 and ECL2 (Fig. 3a-b). The portion of the ECL1 comprising residues
169 N55-Q58 makes contacts with two Cx43 monomers from the opposite membrane, with N55-
170 Q58 of one monomer and Q58'-P59' of the neighboring monomer within 4 Å distance (Fig.
171 3c, *top left*). The ECL2 region that directly participates in sealing the junction includes residues
172 P193-D197. Comparisons of the junction-forming loops in Cx43 to those in Cx46 (Fig. 2c,
173 *middle*) and Cx26 (Fig. 2c, *right*) show that each protein uses a similar pattern of inter-HC
174 interaction within each GJC. It is noteworthy that both the amino acid sequences (Fig. 3d) and
175 the interaction networks (Fig. 3c) are similar in the ECL1 for Cx43 and Cx46, and in the ECL2
176 for Cx46 and Cx26. The differences in these two loops, and especially in ECL2, underlie the
177 inability of Cx43 (which has been grouped into a docking group 2) to engage in heterotypic
178 interactions with group 1 connexins (such as Cx46 and Cx26)²⁷. Our structure is thus in line
179 with the recognized consensus motif necessary for heterotypic complementarity of connixin
180 GJCs²⁸.

181 **Conformation of the Cx43 hemichannel.** Although the two Cx43 GJC structures (in detergent
182 micelles and in nanodiscs) are almost identical, the Cx43 HC shows a notable difference in the
183 ECL1-2 conformation (Fig. 3e-f). The resolution of the HC reconstruction does not allow us to
184 make definitive statements about the orientations of individual side chains, but it is clear that

185 both loops engaging in junction formation move inward upon docking of the two HCs (Fig.
186 3f). This conformational change likely involves intra- and intermolecular cooperativity. The
187 ECL1 and ECL2 are linked via several disulphide bonds, and thus the rearrangement within
188 each molecule would require concerted movement of the whole extracellular domain (ECD).
189 The ECD movement within one monomer is likely cooperatively coupled to the neighboring
190 chains within the Cx43 HC.

191 **Disease-linked mutations in Cx43.** A number of disease-linked mutations associated with
192 Cx43 can be mapped directly to three regions of interest revealed by our structures: (i) the GJC
193 intra-pore lipid-like site, (ii) the ECD, and (iii) the gating region (Fig. 4a). The interior of the
194 channel features two lipid-like densities (Fig. 2h, 4b; Extended Data Fig. 4e, 10a). The
195 observed position of lipid 1 is consistent with the previously found phospholipid-like densities
196 inside the pore of the Cx31.3 HC²⁰. Lipid 2 inserts into the pocket formed by TM1 and TM2,
197 parallel with the NTD. Unlike Cx31.3, where elongated densities within the pore region could
198 be interpreted as hydrophobic tails of bound phospholipids, the density in the Cx43 GJC
199 appears consistent with that of a sterol (Fig. 2h, 4b). The presence of a small hydrophobic small
200 molecule in Cx43 at this site suggests a potential mechanism of lipid-based Cx43 regulation,
201 whereby binding of a lipid could directly influence the conformation of the gating elements of
202 the protein (such as NTD). An effect of a cholesterol analogue 7-ketocholesterol on Cx43
203 permeability has been observed previously²⁹, and such an effect may be mediated via the
204 binding sites within the GJC (or HC) pore (Fig. 4b; Extended Data Fig. 10a). The presence
205 nearby of several residues known to be linked to ODDD when mutated (S27P, I31M³⁰, S86Y³¹,
206 L90V¹⁰) points to a potential functional significance of the intra-pore lipid binding site.

207 Two known mutations linked to ODDD are located in the Cx43 ECD: P59 in ECL1³² and
208 H194 in ECL2³³. As suggested by the Cx43 GJC structures, these residues are located in
209 conserved regions where any substitution can be expected to cause disruption of the contacts
210 critical for junction formation (Fig. 4c).

211 Multiple mutations in Cx43 associated with ODDD are located in the N-terminus (G2V, D3N,
212 L7V, L11I/P, Y17S, S18P), the TM1 region (G21R, G22E, K23T) and the TM2 region
213 proximal to the gate (V96M/E/A, Y98C, K102N)¹¹. In some cases, the mutations reduce the
214 ability of Cx43 to form the gap junction plaques at the plasma membrane, as is the case for
215 Y17S or G21R (as well as L90V, located at the pore lipid binding site)³⁴. The mutations tend
216 to have deleterious effects on the permeability of Cx43 to ions and small molecules¹¹. The
217 mutations G2V, D3N, W4A and L7V were shown to eliminate the function of Cx43 GJCs³⁵.
218 Interestingly, a G8V amino acid substitution has been linked to palmoplantar keratoderma and
219 congenital alopecia 1 (PPKCA1). This mutant can form functional gap junctions and has
220 enhanced HC activity³⁶. Mapping these sites on the structure of Cx43 allows us to gain insights
221 into the possible mechanisms that underlie the associated disorders (Fig. 4d-e). For example,
222 channel blockage or hyperpermeability due to mutations in or around the gating region may
223 link Cx43 to diseases.

224 **Molecular dynamics simulations of Cx43 GJC.** Based on our model of Cx43, the dimensions
225 of the pore opening are likely incompatible with the translocation of a larger molecule, such as
226 ATP, cAMP or IP3 (typical substrates of Cx43 GJC-mediated transport). To assess the
227 permeability of the gate to ions, we performed MD simulations. We performed eighteen
228 independent molecular dynamics simulations of the Cx43 GJC embedded in a double POPC
229 bilayer solvated in 150 mM KCl. Given the ambiguity in the lipid identity and binding mode,
230 in the first set of simulations, no potential lipid surrogates were included inside the pore or
231 NTD region. After equilibration (detailed in Materials and Methods) the dodecameric structure
232 was stable in all simulations, as indicated by the small root mean square deviation (RMSD,
233 Extended Data Fig. 11 a,d).

234 The pore opening has a solvent-accessible radius of ~6 Å (Figure 5c) very close to the effective
235 hydrated radius of K⁺ (~6.6 Å) and Cl⁻ (~7.2 Å). This makes it the most narrow pore opening
236 observed for a connexin channel to date (a comparison of the pore openings in the cryo-EM
237 structures of connexin channels is shown in Extended Data Fig. 12). The NTD regions of Cx43
238 are flexible (Extended Data Fig. 13) and can move laterally and vertically (Movie 1), allowing
239 the passage of ions. The charge distribution inside Cx43 resembles that of the other GJCs^{18,19,37}
240 with a positive electrostatic potential in the NTD region of both HCs within a channel and a
241 negative/neutral region near the HC interface (Fig. 5c). When no transmembrane potential is
242 applied (0 mV, Fig. 5b), Cl⁻ ions accumulate in the NTD regions of Cx43 GJC (anion density
243 peaks in the NTD region) as previously observed for Cx31.3³⁷. At 0 mV, there is an entry
244 barrier of ~3.38 kcal/mol for cations (K⁺) in the NTD region of both HCs (Figure 5d) which is
245 slightly higher than previously reported PMFs values for other homomeric GJCs (Cx46/50)¹⁸.
246 Conversely, anions can permeate the NTD region barrierless (Figure 5d), but they face a higher
247 barrier ~3.84 kcal/mol below this region where the electrostatic potential of the channel is
248 negative, as observed for other GJC¹⁸. Because the NTD domains are flexible, but they do not
249 fully fold inwards, most ions enter and exit the same HC (Extended Data Table 2). Application
250 of a transjunctional voltage lowers the barrier on one HC increasing the number of permeation
251 events. Very few full transjunctional permeation events were observed during the simulations
252 with any applied voltage.

253 As mentioned before, the GJC did not fully open in any of our simulations, i.e., a conformation
254 with all NTDs within the channel symmetrically moving to open the pore was not established
255 at any point. To illustrate this effect, we calculated the root-mean-square deviation for each
256 NTD domain in all simulations (Extended Data Fig. 13). Only at high applied transjunctional
257 voltages only one NTD domain adopted a fully open folded inward conformation (Extended
258 Data Fig. 13).

259 The MD simulations in the absence of a bound ligand reveal an intermediate, metastable state
260 in which ions can permeate from both HCs with similar free-energy barriers and full
261 transjunctional permeations are very rare events. The GJC selectivity and conductance
262 properties are modulated by complex mechanisms involving both the steric aperture and the
263 unique pattern of electrostatic features. In our case, the electrostatic properties of the channel
264 are similar to those published for the Cx46/50 channels¹⁸, but the steric contribution of the
265 NTD region is significantly higher, increasing the barrier for K⁺, resulting in smaller ΔΔG
266 differences than those observed for the open channel (Cx46/50). Other MD studies have shown
267 similar energy barriers for ions¹⁸, leading to entry events but very rare full translocations on
268 the molecular dynamics timescale. Therefore, in the absence of the ligand the channel may
269 exhibit a low residual conductance, as described experimentally³⁸.

270 Despite not knowing the precise identity of the lipid-N, we performed nine MD simulations of
271 the Cx43 HC with a DHEA molecule as a lipid-N surrogate bound between the adjacent chains
272 (Fig. 5e, Extended Data Fig. 14a,b, Movie 2), to understand whether the channel is closed in
273 the presence of the lipid molecule. As expected, even when applying high transmembrane
274 voltage the ion density for both species, K⁺ and Cl⁻, in the NTD region remained zero and no
275 permeation events were observed (Fig. 5e, Extended Data Fig. 14c). Hence, the presence of the
276 bound lipid-N molecule seals the channel by rigidifying the NTD domains.

277

278 Discussion

279 The structures of Cx43 we have obtained by cryo-EM reveal a novel conformation of a
280 connexin channel (both GJC and HC) featuring a closed molecular gate. The state is distinct
281 from the previously observed structures of connexin GJCs and HCs, adding an important
282 missing component to our understanding of connexin-mediated intercellular communication.

283 With these structures in mind, we can now establish the existence of several structurally
284 defined gating substates of the connexin channels: (i) a fully open gate, (ii) a semi-permeable
285 central gate, and (iii) a closed gate (Fig. 6). The gating mechanisms of connexin HCs and GJC
286 are complex and involve multiple components. The available evidence indicates that connexin
287 channels are gated by membrane potential (V_m), by transjunctional potential (V_j), as well as by
288 a range of chemical agents such as pH, Ca^{2+} and organic molecules³⁸. For example, a ball-and-
289 chain model has been proposed for Cx26, whereby at low pH the NTDs extend deep into the
290 pore and occlude the substrate translocation pathway³⁹. This conformation is distinct from the
291 one captured by our cryo-EM reconstructions, and it is possible that under certain conditions
292 the Cx43 NTD may transition from the observed conformation to a low pH Cx26-like state. It
293 is worth mentioning that for the Cx43 HCs the open probability has been shown to be very low
294⁴⁰, and thus a closed conformation such as the one described here may represent the
295 predominant state of the channel.

296 The cytosolic surface of the gate in our structures is positively charged, indicating that specific
297 interaction with anions may be relevant to some of the gating events. As Cx43 is capable of
298 cation and anion permeation⁴¹, the presence of the positively charged surface in this region
299 does not indicate ion selectivity. The differences in the electrostatic properties of the gates and
300 the pore regions in different connexin channels may reflect the differences in their selectivity
301 for ions and small molecules (Extended Data Fig. 12). However, it is also likely that the
302 unstructured regions in Cx43 and other connexins, including the intracellular loop and the C-
303 terminal domain, contribute to the electrostatic potential, substrate selectivity and regulation of
304 these channels. These domains are known to play important roles in connexin channel
305 regulation⁴². However, as these regions are unresolved in any of the available 3D
306 reconstructions of connexin channels, the structural basis of their action remains to be
307 determined.

308 The observation of lipid-like molecules bound inside the pore is intriguing. The use of
309 detergents and lipids is currently a prerequisite for structural analysis of membrane proteins,
310 and it is possible that under solubilization conditions the abundance of added detergent and
311 lipid (CHS) forces the protein to interact with these molecules. Nevertheless, these interactions
312 may correspond to the naturally occurring interactions with the endogenous lipids present in
313 the lipid bilayer of the cell. The presence of such molecules could have important implications
314 for HC or GJC assembly, substrate permeation and molecular gating. It remains to be
315 determined whether Cx43 or other connexin channels harbour intra-pore lipids in the cellular
316 membranes *in vivo*.

317 Distinct gating modes have been shown in the literature for both Cx43 HCs and GJCs, with
318 fast transitions from an open state to a state of residual conductance, and slow transitions from
319 an open to a fully closed state³⁸. The structures of Cx43 described here may represent the
320 closed states, based on the cryo-EM- and MD simulation-based evidence. The closed state
321 could be stabilized by a yet unknown agent that occupies the NTD lipid site formed by the
322 arrangement of the NTDs and TM2 regions observed in our structures. It is worth noting that
323 the majority of Cx43 channels in a GJ plaque are closed, with only a small fraction of the
324 channels active⁴³. Detailed investigations of Cx43 and other connexin channels will be
325 required to determine whether the gate conformation observed here is a common feature among
326 different GJCs and HCs, and to pinpoint the physiological circumstances that establish this
327 gating conformation. Finally, capturing the structures of Cx43 channels in distinct
328 conformations under a wide range of physiologically relevant conditions will be required to
329 establish its mechanism of action, gating and regulation.

330

331 **Acknowledgements**

332 We thank Emiliya Poghossian (EM Facility, PSI) and Miroslav Peterek (ScopeM, ETH Zurich)
333 for expert support in cryo-EM data collection. We also thank Spencer Bliven and Marc Caubet-
334 Serrabou (PSI) for the support in high performance computing. The work was supported by a
335 grant from Horten Foundation, and by the Swiss National Science Foundation grant 184951
336 (VMK). FLG and SAG thank the CSCS and PRACE for supercomputing resources (projects
337 pr126 and s1107).

338

339 **Competing interests**

340 Authors declare that they have no competing interests.

341

342 **Data and materials availability**

343 The atomic coordinates and structure factors have been deposited in the Protein Data Bank
344 (7Z1T, 7Z22, 7Z23); the density maps have been deposited in the Electron Microscopy Data
345 Bank (EMD-14452, EMD-14455, EMD-14456). The mass spectrometry data have been
346 deposited at ProteomeXChange via PRIDE (PXD033824). The MD trajectories will be
347 uploaded to Zenodo. All other data are available in the main text or the supplementary
348 materials.

349

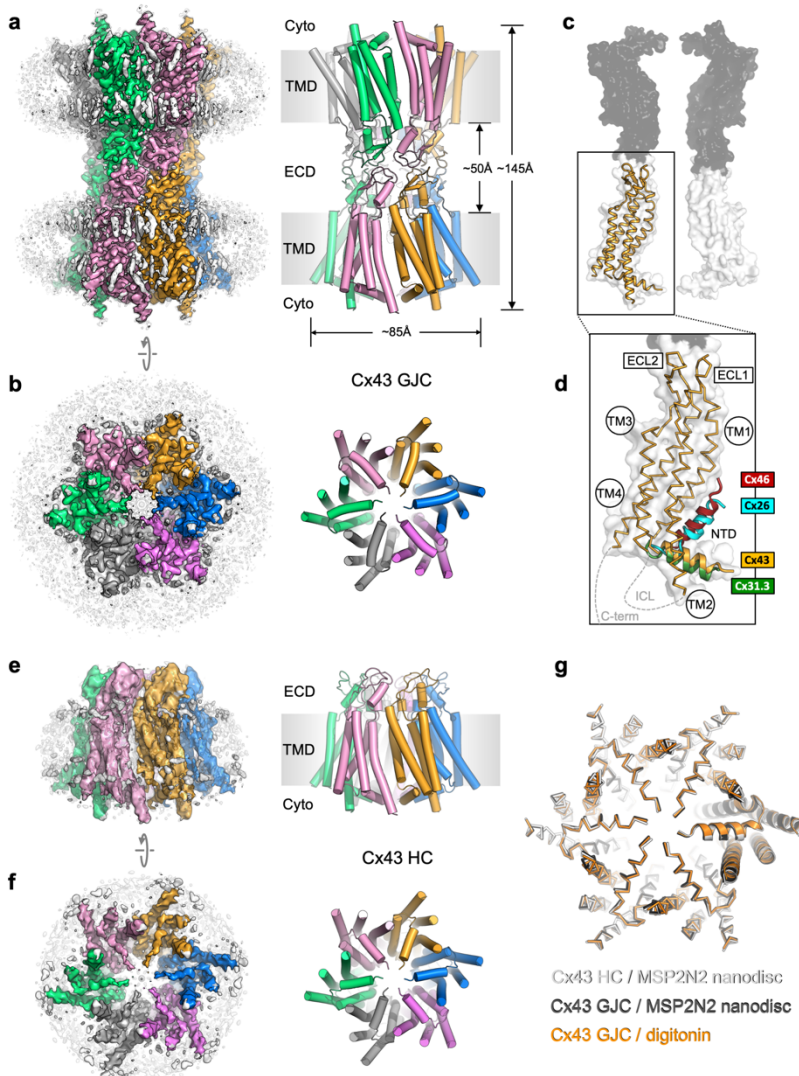
350 **Author contributions**

351 C.Q. planned and performed the experiments, analyzed the data, wrote the manuscript, S.A.G.
352 planned, performed and analyzed the simulations, co-wrote the manuscript, P.L. performed the
353 experiments, co-wrote the manuscript, A.O. performed the experiments, analyzed the data,
354 D.L.P. performed the experiments, analyzed the data, E.B. performed the experiments,
355 analyzed the data, D.S. performed the experiments, analysed the data, co-wrote the manuscript,
356 P.P. provided the reagents, equipment and expertise for mass spectrometry experiments, N.Z.
357 provided the reagents, equipment and expertise for lipidomics analysis, M.B. planned the
358 experiments, analyzed the data, co-wrote the manuscript, F.L.G. planned and analyzed the
359 simulations, co-wrote the manuscript, V.M.K. planned and performed the experiments,
360 analyzed the data, wrote the manuscript.

361

362
363
364

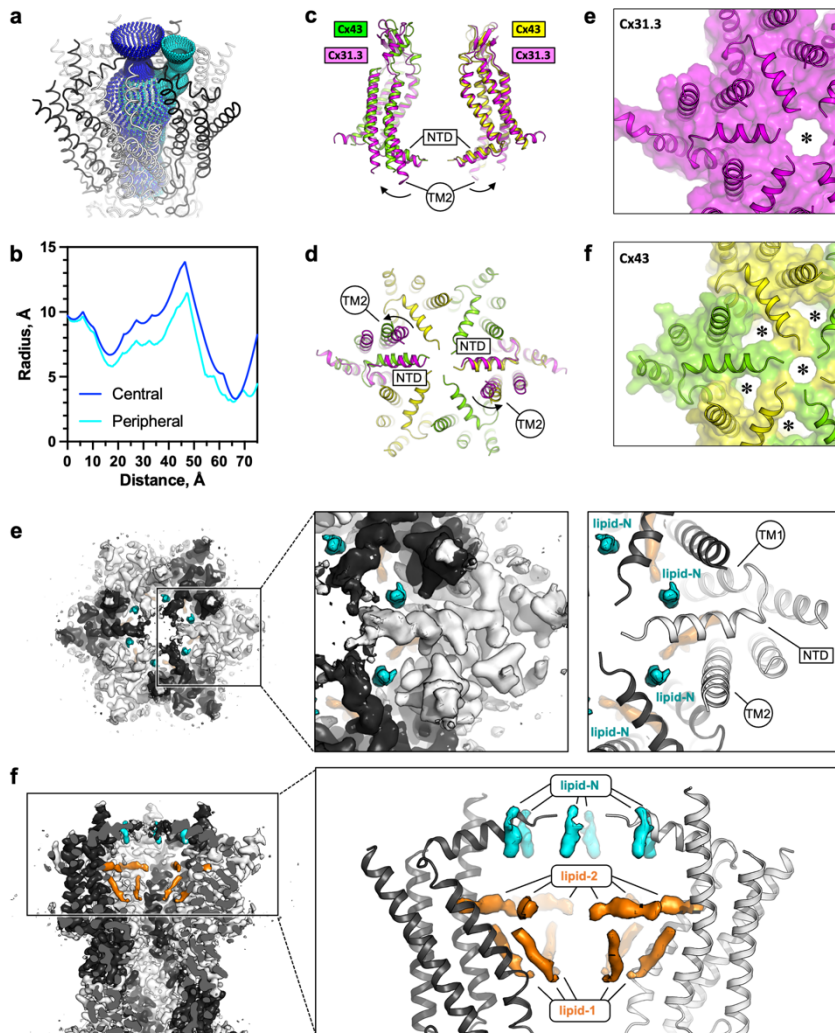
Figures



365
366

Figure 1. Structure of human Cx43 gap junction channel. a-b, Cryo-EM density map and model of Cx43 GJC solved by cryo-EM at 2.26 Å resolution. The individual Cx43 monomers in each HC within the GJC are coloured blue, pink, grey, green, salmon and orange. Grey densities correspond to the detergent micelle and the bound sterol-like molecules. **c,** The position of a single Cx43 monomer (orange) within a GJC (represented as a surface of juxtaposed Cx43 monomers in two distinct membrane regions, white and grey). **d,** Alignment of the monomers of Cx43, Cx26 (PDB ID: 2zw3), Cx46 (PDB ID: 7jkc) and Cx31.3 (PDB ID: 6l3t) shows the distinct orientations of the N-terminal domain (“NTD”) helix. Individual TM domains, extracellular loops 1 and 2 (“ECL1-2”), relative positions of the intracellular loop (“ICL”) and the C-terminus (“C-term”) are indicated. **e-f,** Same as a-b, for the Cx43 HC in MSP2N2 nanodiscs at 3.98 Å resolution. **g,** Alignment of three indicated structures shows that the conformation of the gating region is highly conserved. The models are shown as ribbons; one of the aligned monomers in each of the structures is represented as cartoon, to clearly indicate the monomer boundaries.

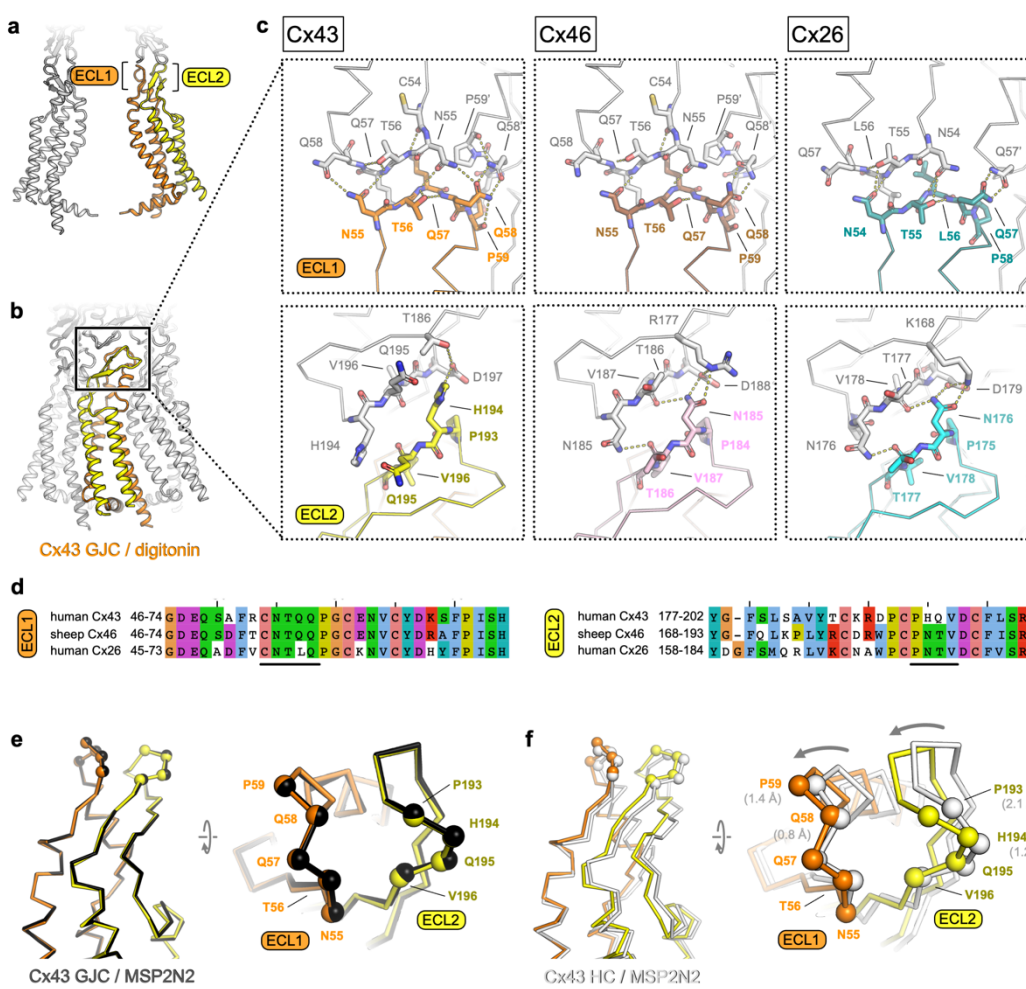
381
382



383
384

385 **Figure 2. The Cx43 gate adopts a closed conformation. a-b,** Analysis of the pore opening
386 dimensions using HOLE reveals a constriction of the pore in the gate region. Only a central
387 opening and one of the six peripheral openings within one HC of Cx43 GJC in digitonin is
388 shown. The distance is calculated from the center of the GJC pore to a point outside of the
389 channel. Central and peripheral openings are coloured blue and cyan, respectively. **c-d,**
390 Comparison of the Cx43 in digitonin with the Cx31.3 HC shows that the peripheral opening is
391 created by the particular arrangement of the NTD and by adjustment of the TM2. **e-f,** The
392 distinct NTD/TM2 arrangement results in a single pore opening in the structure of Cx31.3
393 (indicated with an asterisk, e), contrary to Cx43 (f). **g,** A view of the Cx43 gating region from
394 the cytosol reveals the location of the “lipid-N” molecules stabilizing the NTD arrangement,
395 shown as isolated densities (cyan). **h,** A slab view of the gating region parallel to the membrane
396 plane shows the relative arrangement of the lipid-N and the intra-pore lipid densities (“lipid-
397 1” and lipid-2”; orange).

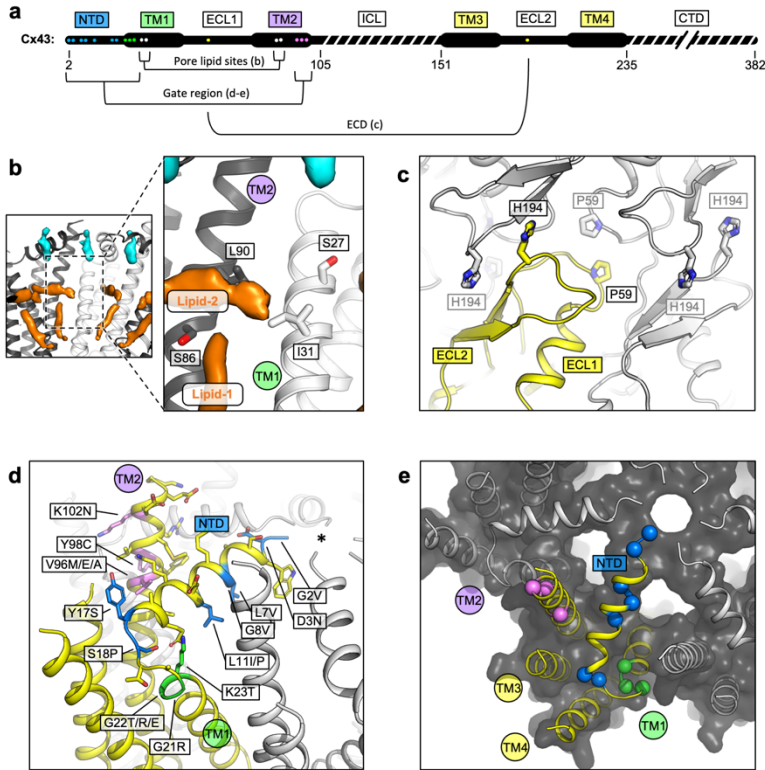
398



399
400

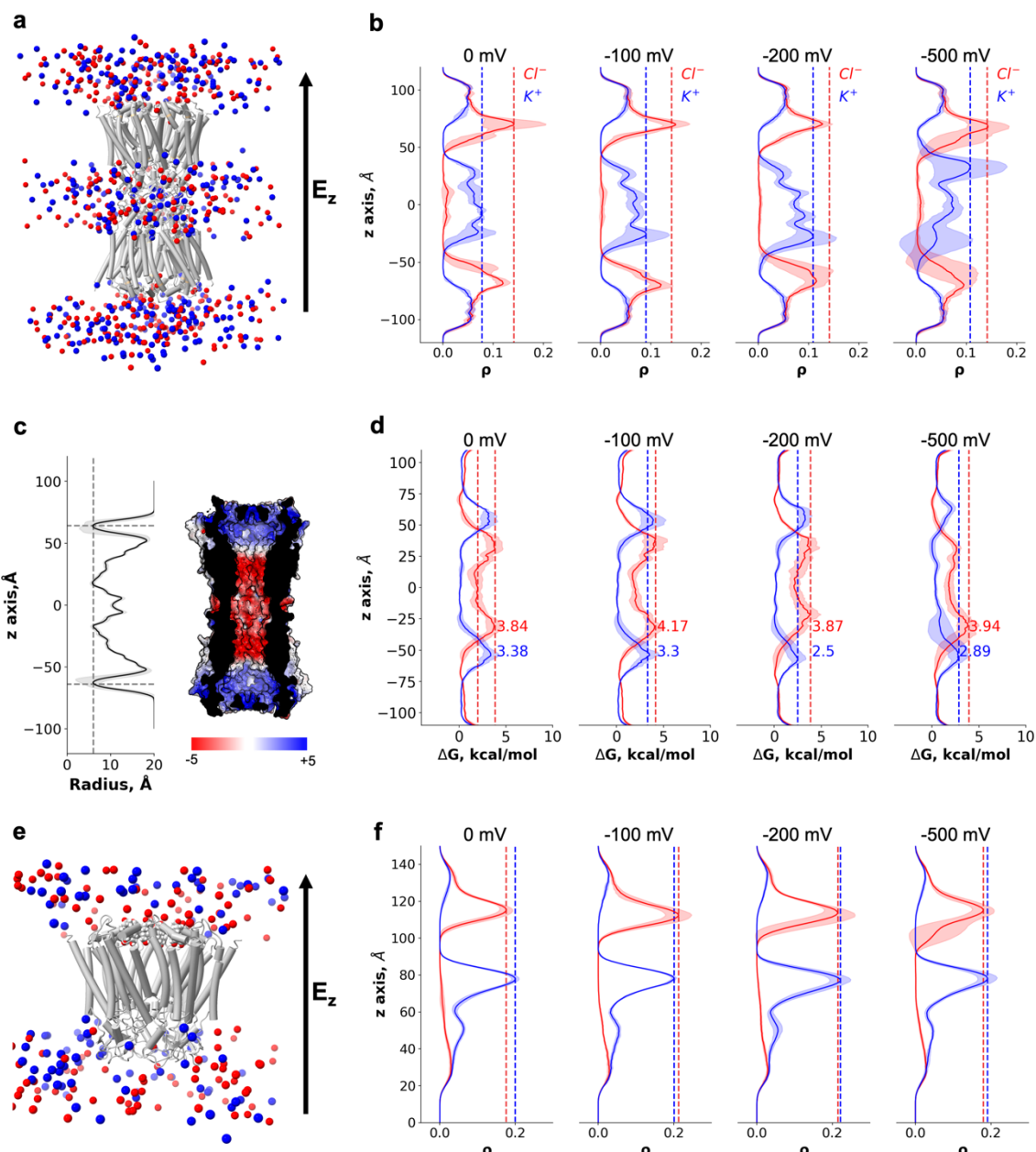
Figure 3. Extracellular domain of Cx43 GJC and HC. **a-b**, The lateral views of Cx43 GJC in digitonin, indicating the positions of the extracellular loops 1 and 2. **c**, Views of the extracellular loops ECL1 (top) and ECL2 (bottom), for Cx43 (left), Cx46, (middle; PDB ID: 7jkc), and Cx26 (right; PDB ID: 2zw3). The residues of one monomer in each of the structures, directly involved in junction formation, are coloured by element with carbon atoms as orange/yellow (Cx43), brown/pink (Cx46) and teal/cyan (Cx26). The residues of the neighbouring connexin monomers within 4 Å distance are shown coloured with white carbon atoms. Dotted lines indicate electrostatic contacts, calculated in PyMol. **d**, Sequence alignment of the complete ECL1 and ECL2 regions of the three proteins shown in c. The black lines indicate the GJC interface residues, as shown in c. **e**, Alignment of the Cx43 GJC structures in digitonin micelles and in nanodiscs. Cα atoms of the interface residues shown in C are represented as spheres (the ribbon and spheres of Cx43 in nanodiscs is coloured black). **f**, Same as e, for a comparison between Cx43 GJC in digitonin and Cx43 HC in nanodiscs. The arrow indicates the movement of the two loops that accompanies GJC formation. The ribbon and spheres of Cx43 HC are light grey. The grey numbers in brackets indicate displacement of selected Cα atoms (residues P59, Q58, P193, P194).

416
417



418
419
420
421
422
423
424
425
426
427
428
429
430
431
432
433

Figure 4. Locations of the disease-linked mutations in the Cx43 GJC structure. **a**, Disease-linked mutations mapped on the sequence of Cx43. The amino acid residues proximal to the intrapore lipid densities (“Pore lipid sites”) are shown as white dots. The residues at the GJC interface are shown as yellow dots (“ECD”). The residues of the gating region (“Gate region”) are shown as blue (NTD), green (TM1) and violet (TM2) dots. The sequence elements not resolved in our 3D reconstruction are indicated with a dashed line. **b**, Two sterol-like density elements (lipid-1 and -2) are located within the pore region of Cx43 GJC (white). The indicated disease-linked mutations are located within close distance of the pore lipid densities. **c**, A view of the extracellular loops forming the junction, indicating two residues known to be linked with ODDD, P59 and H194 (side chains shown as sticks; one of the monomers in the GJC is coloured yellow). **d**, A view of the gating region with the highlighted disease-linked mutations, colored as in a. **e**, A similar representation of the disease-linked mutations, with C α atoms shown as spheres, illustrating the contribution of the mutants to gate formation.

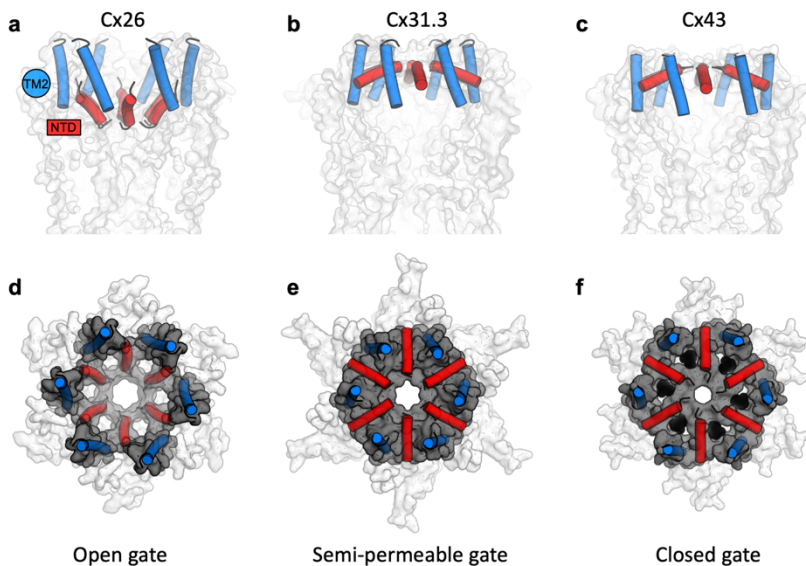


434
435

436 **Figure 5. Molecular dynamics simulations of the Cx43 GJC and HC.** **a**, Cartoon
437 representation of the double-bilayer system including the GJC (cartoon) and ions (vdw
438 spheres). Lipidic membrane and water residues have been removed for clarity. The direction
439 of the applied constant electric field, E_z , is indicated with an arrow. **b**, Ion density (ρ) profiles
440 (average and fluctuations) along the diffusion axis of the GJC coloured in red for anions and
441 blue for cations, for the simulated applied transjunctional voltages. **c**, The solvent-accessible
442 radius (and fluctuations during MD) along the diffusion axis of the GJC. The dotted lines
443 correspond to the minimum radius and the position of the NTD regions. The surface
444 representation of Cx43 is coloured according to the calculated electrostatic potential; the slab
445 view shows the properties of the pore. **d**, Average free energy experienced (at least two
446 simulation replicates per panel) by the K^+ (blue) and Cl^- (red) while permeating the pore with
447 different applied transmembrane potential (from right to left: 0 mV, -100 mV, -200 mV and
448 -500 mV). The dotted lines correspond to the maximum free energy barrier for anions (red) and
449 cations (blue). **e**, Cartoon representation of the lipid-bound system including the HC (cartoon)
450 and ions (vdw spheres). Lipidic membrane and water residues have been removed for clarity.
451 The direction of the applied constant electric field, E_z , is indicated with an arrow. **f**, Ion density

452 (ρ) profiles (average and fluctuations) along the diffusion axis of the HC coloured in red for
453 anions and blue for cations, for the simulated applied transmembrane voltages.
454

455



456

457

458 **Figure 6. A structure-based view of connexin gating states.** **a**, The side view of a fully open
459 gate, as observed in Cx26 GJC (PDB ID: 2zw3); the gate-forming regions of the protein, NTD
460 (red) and TM2 (blue), are shown as cylinders. Similar arrangement of the gating elements has
461 been observed in Cx46/Cx50. This conformation of the gate is permeable to a wide range of
462 substrates, including small molecules and ions. **b**, The semi-permeable central gate is featured
463 in the structure of Cx31.3 HC (PDB ID: 6l3t). In this conformation the gate is likely selective
464 for ions (Cx31.3 has been shown to have a preference for anions), based on the dimensions of
465 the gate. **c**, The closed gate is featured in the Cx43 structures (here, the Cx43 in digitonin is
466 shown as an example). **d-f**, Same as a-c, viewed from the cytosolic side of the channel. The
467 gray surface corresponds to the NTD and TM2 regions; the white surface corresponds to the
468 rest of the protein; lipid-N molecules in f are shown as black spheres, using a model of DHEA
469 manually placed into the six NTD lipid site regions for illustration purposes (the exact identity
470 of the lipid-N molecule is unknown).

471

472 **References**

- 473
- 474 1 Churko, J. M. & Laird, D. W. Gap junction remodeling in skin repair following
475 wounding and disease. *Physiology (Bethesda)* **28**, 190-198 (2013).
<https://doi.org/10.1152/physiol.00058.2012>
- 476
- 477 2 Liang, Z. *et al.* The Multifaceted Role of Astrocyte Connexin 43 in Ischemic Stroke
478 Through Forming Hemichannels and Gap Junctions. *Front Neurol* **11**, 703 (2020).
<https://doi.org/10.3389/fneur.2020.00703>
- 479
- 480 3 Poelzing, S. & Rosenbaum, D. S. Altered connexin43 expression produces arrhythmia
481 substrate in heart failure. *Am J Physiol Heart Circ Physiol* **287**, H1762-1770 (2004).
<https://doi.org/10.1152/ajpheart.00346.2004>
- 482
- 483 4 Rodriguez-Sinovas, A., Sanchez, J. A., Valls-Lacalle, L., Consegal, M. & Ferreira-
484 Gonzalez, I. Connexins in the Heart: Regulation, Function and Involvement in Cardiac
485 Disease. *Int J Mol Sci* **22** (2021). <https://doi.org/10.3390/ijms22094413>
- 486 5 Syrjanen, J., Michalski, K., Kawate, T. & Furukawa, H. On the molecular nature of
487 large-pore channels. *J Mol Biol*, 166994 (2021).
<https://doi.org/10.1016/j.jmb.2021.166994>
- 488
- 489 6 Srinivas, M., Verselis, V. K. & White, T. W. Human diseases associated with connexin
490 mutations. *Biochim Biophys Acta Biomembr* **1860**, 192-201 (2018).
<https://doi.org/10.1016/j.bbamem.2017.04.024>
- 491
- 492 7 Beyer, E. C., Paul, D. L. & Goodenough, D. A. Connexin43: a protein from rat heart
493 homologous to a gap junction protein from liver. *J Cell Biol* **105**, 2621-2629 (1987).
<https://doi.org/10.1083/jcb.105.6.2621>
- 494
- 495 8 Robertson, J. D. The Occurrence of a Subunit Pattern in the Unit Membranes of Club
496 Endings in Mauthner Cell Synapses in Goldfish Brains. *J Cell Biol* **19**, 201-221 (1963).
<https://doi.org/10.1083/jcb.19.1.201>
- 497
- 498 9 Laird, D. W. & Lampe, P. D. Therapeutic strategies targeting connexins. *Nat Rev Drug
499 Discov* **17**, 905-921 (2018). <https://doi.org/10.1038/nrd.2018.138>
- 500 10 Paznekas, W. A. *et al.* Connexin 43 (GJA1) mutations cause the pleiotropic phenotype
501 of oculodentodigital dysplasia. *Am J Hum Genet* **72**, 408-418 (2003).
<https://doi.org/10.1086/346090>
- 502
- 503 11 Paznekas, W. A. *et al.* GJA1 mutations, variants, and connexin 43 dysfunction as it
504 relates to the oculodentodigital dysplasia phenotype. *Hum Mutat* **30**, 724-733
505 (2009). <https://doi.org/10.1002/humu.20958>
- 506
- 507 12 Wiest, T. *et al.* Clinical and genetic variability of oculodentodigital dysplasia. *Clin
508 Genet* **70**, 71-72 (2006). <https://doi.org/10.1111/j.1399-0004.2006.00631.x>
- 509
- 510 13 Dasgupta, C. *et al.* Identification of connexin43 (alpha1) gap junction gene mutations
511 in patients with hypoplastic left heart syndrome by denaturing gradient gel
512 electrophoresis (DGGE). *Mutat Res* **479**, 173-186 (2001).
[https://doi.org/10.1016/s0027-5107\(01\)00160-9](https://doi.org/10.1016/s0027-5107(01)00160-9)
- 513
- 514 14 Pizzuti, A. *et al.* A homozygous GJA1 gene mutation causes a Hallermann-
515 Streiff/ODDD spectrum phenotype. *Hum Mutat* **23**, 286 (2004).
<https://doi.org/10.1002/humu.9220>
- 516
- 517 15 Ribeiro-Rodrigues, T. M., Martins-Marques, T., Morel, S., Kwak, B. R. & Girao, H. Role
518 of connexin 43 in different forms of intercellular communication - gap junctions,
519 extracellular vesicles and tunnelling nanotubes. *J Cell Sci* **130**, 3619-3630 (2017).
<https://doi.org/10.1242/jcs.200667>

- 519 16 Unger, V. M., Kumar, N. M., Gilula, N. B. & Yeager, M. Three-dimensional structure of
520 a recombinant gap junction membrane channel. *Science* **283**, 1176-1180 (1999).
521 <https://doi.org/10.1126/science.283.5405.1176>
- 522 17 Maeda, S. *et al.* Structure of the connexin 26 gap junction channel at 3.5 Å
523 resolution. *Nature* **458**, 597-602 (2009). <https://doi.org/10.1038/nature07869>
- 524 18 Myers, J. B. *et al.* Structure of native lens connexin 46/50 intercellular channels by
525 cryo-EM. *Nature* **564**, 372-377 (2018). <https://doi.org/10.1038/s41586-018-0786-7>
- 526 19 Flores, J. A. *et al.* Connexin-46/50 in a dynamic lipid environment resolved by
527 CryoEM at 1.9 Å. *Nat Commun* **11**, 4331 (2020). <https://doi.org/10.1038/s41467-020-18120-5>
- 529 20 Lee, H. J. *et al.* Cryo-EM structure of human Cx31.3/GJC3 connexin hemichannel. *Sci
530 Adv* **6**, eaba4996 (2020). <https://doi.org/10.1126/sciadv.aba4996>
- 531 21 Xu, Q. *et al.* Gating of connexin 43 gap junctions by a cytoplasmic loop calmodulin
532 binding domain. *Am J Physiol Cell Physiol* **302**, C1548-1556 (2012).
<https://doi.org/10.1152/ajpcell.00319.2011>
- 534 22 Ponsaerts, R. *et al.* Intramolecular loop/tail interactions are essential for connexin
535 43-hemichannel activity. *FASEB J* **24**, 4378-4395 (2010).
<https://doi.org/10.1096/fj.09-153007>
- 537 23 Khan, A. K., Jagielnicki, M., Bennett, B. C., Purdy, M. D. & Yeager, M. Cryo-EM
538 structure of an open conformation of a gap junction hemichannel in lipid bilayer
539 nanodiscs. *Structure* **29**, 1040-1047 e1043 (2021).
<https://doi.org/10.1016/j.str.2021.05.010>
- 541 24 Bennett, B. C. *et al.* An electrostatic mechanism for Ca(2+)-mediated regulation of
542 gap junction channels. *Nat Commun* **7**, 8770 (2016).
<https://doi.org/10.1038/ncomms9770>
- 544 25 Gartside, S. E., Griffith, N. C., Kaura, V. & Ingram, C. D. The neurosteroid
545 dehydroepiandrosterone (DHEA) and its metabolites alter 5-HT neuronal activity via
546 modulation of GABA_A receptors. *J Psychopharmacol* **24**, 1717-1724 (2010).
<https://doi.org/10.1177/0269881109105836>
- 548 26 Kimonides, V. G., Khatibi, N. H., Svendsen, C. N., Sofroniew, M. V. & Herbert, J.
549 Dehydroepiandrosterone (DHEA) and DHEA-sulfate (DHEAS) protect hippocampal
550 neurons against excitatory amino acid-induced neurotoxicity. *Proc Natl Acad Sci U S
551 A* **95**, 1852-1857 (1998). <https://doi.org/10.1073/pnas.95.4.1852>
- 552 27 Bai, D., Yue, B. & Aoyama, H. Crucial motifs and residues in the extracellular loops
553 influence the formation and specificity of connexin docking. *Biochim Biophys Acta
554 Biomembr* **1860**, 9-21 (2018). <https://doi.org/10.1016/j.bbamem.2017.07.003>
- 555 28 Koval, M., Molina, S. A. & Burt, J. M. Mix and match: investigating heteromeric and
556 heterotypic gap junction channels in model systems and native tissues. *FEBS Lett
557* **588**, 1193-1204 (2014). <https://doi.org/10.1016/j.febslet.2014.02.025>
- 558 29 Girao, H., Catarino, S. & Pereira, P. 7-Ketocholesterol modulates intercellular
559 communication through gap-junction in bovine lens epithelial cells. *Cell Commun
560 Signal* **2**, 2 (2004). <https://doi.org/10.1186/1478-811X-2-2>
- 561 30 Richardson, R., Donnai, D., Meire, F. & Dixon, M. J. Expression of Gja1 correlates with
562 the phenotype observed in oculodentodigital syndrome/type III syndactyly. *J Med
563 Genet* **41**, 60-67 (2004). <https://doi.org/10.1136/jmg.2003.012005>
- 564 31 Jamsheer, A. *et al.* Three novel GJA1 missense substitutions resulting in oculo-dento-
565 digital dysplasia (ODDD) - further extension of the mutational spectrum. *Gene* **539**,
566 157-161 (2014). <https://doi.org/10.1016/j.gene.2014.01.066>

- 567 32 Vasconcellos, J. P. *et al.* A novel mutation in the GJA1 gene in a family with
568 oculodentodigital dysplasia. *Arch Ophthalmol* **123**, 1422-1426 (2005).
569 <https://doi.org/10.1001/archopht.123.10.1422>
- 570 33 Vitiello, C. *et al.* A novel GJA1 mutation causes oculodentodigital dysplasia without
571 syndactyly. *Am J Med Genet A* **133A**, 58-60 (2005).
572 <https://doi.org/10.1002/ajmg.a.30554>
- 573 34 Lai, A. *et al.* Oculodentodigital dysplasia connexin43 mutations result in non-
574 functional connexin hemichannels and gap junctions in C6 glioma cells. *J Cell Sci* **119**,
575 532-541 (2006). <https://doi.org/10.1242/jcs.02770>
- 576 35 Shao, Q. *et al.* Structure and functional studies of N-terminal Cx43 mutants linked to
577 oculodentodigital dysplasia. *Mol Biol Cell* **23**, 3312-3321 (2012).
578 <https://doi.org/10.1091/mbc.E12-02-0128>
- 579 36 Wang, H. *et al.* Exome sequencing reveals mutation in GJA1 as a cause of
580 keratoderma-hypotrichosis-leukonychia totalis syndrome. *Hum Mol Genet* **24**, 243-
581 250 (2015). <https://doi.org/10.1093/hmg/ddu442>
- 582 37 Hyuk-Joon Lee, H. J., Jaekyung Hyun, Bumhan Ryu, Kunwoong Park, Hyun-Ho Lim,
583 Jejoong Yoo, Jae-Sung Woo. Cryo-EM structure of human Cx31.3/GJC3 connexin
584 hemichannel. *Science Advances* **6** (2020).
- 585 38 Bukauskas, F. F. & Verselis, V. K. Gap junction channel gating. *Biochim Biophys Acta*
586 **1662**, 42-60 (2004). <https://doi.org/10.1016/j.bbamem.2004.01.008>
- 587 39 Khan, A. K. *et al.* A Steric "Ball-and-Chain" Mechanism for pH-Mediated Regulation of
588 Gap Junction Channels. *Cell Rep* **31**, 107482 (2020).
589 <https://doi.org/10.1016/j.celrep.2020.03.046>
- 590 40 Contreras, J. E., Saez, J. C., Bukauskas, F. F. & Bennett, M. V. Gating and regulation of
591 connexin 43 (Cx43) hemichannels. *Proc Natl Acad Sci U S A* **100**, 11388-11393 (2003).
592 <https://doi.org/10.1073/pnas.1434298100>
- 593 41 Wang, H. Z. & Veenstra, R. D. Monovalent ion selectivity sequences of the rat
594 connexin43 gap junction channel. *J Gen Physiol* **109**, 491-507 (1997).
595 <https://doi.org/10.1085/jgp.109.4.491>
- 596 42 D'Hondt, C., Iyyathurai, J., Himpens, B., Leybaert, L. & Bultynck, G. Cx43-hemichannel
597 function and regulation in physiology and pathophysiology: insights from the bovine
598 corneal endothelial cell system and beyond. *Front Physiol* **5**, 348 (2014).
599 <https://doi.org/10.3389/fphys.2014.00348>
- 600 43 Bukauskas, F. F. *et al.* Clustering of connexin 43-enhanced green fluorescent protein
601 gap junction channels and functional coupling in living cells. *Proc Natl Acad Sci U S A*
602 **97**, 2556-2561 (2000). <https://doi.org/10.1073/pnas.050588497>
- 603